

Symmetry-Constrained Language-Guided Program Synthesis for Discovering Governing Equations from Noisy and Partial Observations

Mirza Samad Ahmed Baig^{1,*} Syeda Anshrah Gillani^{2,†}

¹Fandaqah (Owned by Dyafa), Al Khobar, Eastern Province, Saudi Arabia

²Hamdard University, Karachi, Pakistan

*MirzaSamadcontact@gmail.com

†SyedaAnshrah16@gmail.com

Abstract. Discovering compact governing equations from experimental observations is one of the defining objectives of quantitative science, yet practical discovery pipelines routinely fail when measurements are noisy, relevant state variables are unobserved, or multiple symbolic structures explain the data equally well within statistical uncertainty. Here we introduce SYMLANG (**S**ymmetry-constrained **L**anguage-guided equation discovery), a unified framework that brings together three previously separate ideas: (i) *typed symmetry-constrained grammars* that encode dimensional analysis, group-theoretic invariance, and parity constraints as hard production rules, eliminating on average 71.3% of candidate expression trees before any fitting; (ii) *language-model-guided program synthesis* in which a fine-tuned 7B-parameter proposer, conditioned on interpretable data descriptors, efficiently navigates the constrained search space; and (iii) *MDL-regularized Bayesian model selection* coupled with block-bootstrap stability analysis that quantifies structural uncertainty rather than committing to a single best equation. Across 133 dynamical systems spanning classical mechanics, electrodynamics, thermodynamics, population dynamics, and nonlinear oscillators, SYMLANG achieves an exact structural recovery rate of 83.7% under 10% observational noise, a 22.4 percentage-point improvement over the next-best baseline while reducing out-of-distribution extrapolation error by 61% and near-eliminating conservation-law violations (3.1×10^{-3} vs. 187.3×10^{-3} physical drift for the closest competitor). Under 50% state occlusion, exact recovery reaches 61.2% versus 38.4%. In all tested regimes the framework correctly identifies structural degeneracy, reporting it explicitly, rather than returning a confidently wrong single equation. The framework is fully open-source and reproducible, providing a principled pathway from raw data to interpretable, physically auditable symbolic laws.

Keywords: symbolic regression · equation discovery · symmetry constraints · dimensional analysis · Bayesian model selection · program synthesis · partial observability · structure uncertainty

Introduction

The compression of complex empirical phenomena into compact symbolic laws—Newton’s second law, Maxwell’s equations, the Lotka-Volterra system represents one of science’s most powerful and reproducible achievements. Yet recovering such laws automatically from measured data remains profoundly difficult, particularly when (a) measurements carry substantial noise that corrupts derivative estimates, (b) relevant state variables are unobserved so that only an effective or projected dynamics is accessible, and (c) finite data support observationally equivalent families of symbolic expressions whose discrimination requires targeted experimentation.

Early computational approaches to this problem relied on genetic programming evolved over large symbolic search spaces [7, 1, 8], which are flexible but exponentially expensive and provide no principled uncertainty. A major practical advance came with sparse regression over a fixed operator libraries [2, 23]: by treating equation discovery as ℓ_1 -penalized regression on a rich feature matrix, SINDy [2] and its descendants [20, 22, 21, 24] achieve scalable recovery of low-complexity dynamics. The fundamental limitation of this family is the fixed library assumption: equations outside the library are structurally invisible.

Neural approaches relax the library constraint. Physics-inspired symbolic regression (AI Feynman [3]) exploits dimensional analysis and neural network fitting to recursively

decompose complex expressions. Evolutionary symbolic regression (PySR [4]) uses multi-population evolution with Pareto-front complexity penalization, building on a long line of genetic programming innovations [11, 15, 9, 10]. Deep symbolic regression (DSR [5]) frames expression tree generation as a reinforcement learning problem, while transformer-based and generative approaches model the distribution over expression trees directly [6, 13, 14, 19, 12]. Bayesian symbolic regression [12] explicitly models posterior uncertainty over tree structures, though at considerable computational cost. Inductive process modeling [16] and knowledge-rich discovery systems [18] demonstrate that incorporating prior structural knowledge substantially accelerates convergence. Large language models have recently shown promise as mathematical discovery engines [49, 50].

In parallel, a distinct family of neural models has emerged that respects physical structure without recovering interpretable equations: physics-informed neural networks [25] solve PDEs while satisfying boundary conditions; neural ODEs [26] and universal differential equations [27] learn continuous dynamics in latent space; Hamiltonian [28] and Lagrangian [29] neural networks embed energy conservation architecturally; symplectic integrators [30] preserve phase-space volume; and Fourier Neural Operators [31] and DeepONet [32] learn operator mappings between function spaces. These models predict accurately but are not interpretable in the sense of producing a human-readable symbolic law.

The geometric deep learning programme [34, 35, 38] es-

establishes a principled foundation for incorporating group equivariance into neural architectures. Conservation-law finders [36, 37] can automatically identify conserved quantities from trajectories. Yet neither stream directly produces compact symbolic laws with calibrated structural uncertainty.

Three critical gaps persist across this landscape. **First**, physical constraints, dimensional analysis, parity, rotational invariance, Noether conservation [33] are either ignored entirely or applied only as post-hoc screening, missing the opportunity to prune the hypothesis space *before* search. **Second**, existing methods return a single “best” symbolic expression, providing no principled measure of structural uncertainty: when data support multiple observationally equivalent forms, a single point estimate is epistemically misleading and can cause practitioners to overinterpret finite-sample coincidences as fundamental laws. **Third**, partial observability where some state variables are not measured is handled at best heuristically, despite being ubiquitous in real experimental settings.

We introduce SYMLANG, which directly addresses all three gaps through a modular five-stage pipeline: symmetry-constrained grammar construction; language-guided proposal; differentiable constant fitting; MDL-regularized model selection; and bootstrap stability with identifiability diagnostics. The result is a system that is simultaneously more sample-efficient, more physically consistent, and more epistemically honest than any prior method.

Theoretical Background and Problem Formulation

Dynamical systems and the discovery problem

We consider continuous-time systems of the form

$$\frac{d\mathbf{x}}{dt} = \mathbf{f}(\mathbf{x}(t), \mathbf{u}(t), t; \theta^*), \quad \mathbf{x}(t_0) = \mathbf{x}_0, \quad (1)$$

where $\mathbf{x}(t) \in \mathbb{R}^d$ is the full state vector, $\mathbf{u}(t) \in \mathbb{R}^q$ denotes external control inputs or forcing, and θ^* are unknown scalar parameters (physical constants). The observation model is

$$\mathbf{y}(t_m) = \mathcal{H}(\mathbf{x}(t_m)) + \varepsilon_m, \quad m = 1, \dots, M, \quad (2)$$

where $\mathcal{H} : \mathbb{R}^d \rightarrow \mathbb{R}^{d_o}$ is a potentially non-surjective observation operator ($d_o \leq d$) and $\varepsilon_m \sim \mathcal{N}(\mathbf{0}, \sigma^2 \mathbf{I})$ is i.i.d. Gaussian noise. The *discovery problem* is: given $\{(\mathbf{y}(t_m), \mathbf{u}(t_m))\}_{m=1}^M$, recover a symbolic expression tree e^* representing \mathbf{f} together with calibrated uncertainty over the space of alternative structures.

Expression trees and the grammar formalism

A symbolic expression is represented as an ordered rooted tree $e = (V, E, \ell)$, where each internal node $v \in V$ carries an operator label $\ell(v) \in \mathcal{O}$ (from a fixed operator set: $\{+, -, \times, \div, \sin, \cos, \exp, \log, (\cdot)^n\}$) and each leaf carries a variable, constant, or rational number. The *arity* of an operator determines the number of child branches. The complexity of e is measured by $|e| = |V|$ (number of nodes).

A context-free grammar $\mathcal{G} = (\mathcal{N}, \Sigma, \mathcal{P}, S)$ defines the set of admissible expression trees through production rules \mathcal{P} , where nonterminals \mathcal{N} generate typed subtrees and terminals Σ are leaf tokens. Unconstrained, the number of distinct expression trees of depth $\leq \ell$ grows doubly exponentially in ℓ , motivating the symmetry constraints developed in the next section.

Definition 1 (Type-consistent grammar). *A typed CFG is a grammar \mathcal{G} in which each nonterminal $A \in \mathcal{N}$ carries a type tuple $\tau(A) = (\mathbf{d}_A, p_A, \iota_A)$ where $\mathbf{d}_A \in \mathbb{Z}^5$ is a physical dimension vector (M, L, T, Θ, I) , $p_A \in \{+1, -1, 0\}$ is a parity tag, and ι_A is an invariance class. A production rule $A \rightarrow \alpha$ is type-consistent if the type of α (computed by type propagation rules for each operator) matches $\tau(A)$.*

Proposition 1 (Pruning bound). *Let \mathcal{G}_0 be the unconstrained grammar and \mathcal{G}_c the type-consistent grammar over the same operator set. If f satisfies k independent type constraints, then $|\mathcal{L}(\mathcal{G}_c, \ell)| \leq C^{-k} |\mathcal{L}(\mathcal{G}_0, \ell)|$ for a constant $C > 1$ depending on the operator branching structure.*

Empirically, we measure $C^k \approx 3.5$ on average across the 133-system benchmark, corresponding to the 71.3% pruning rate at depth $\ell \leq 12$.

The SymLang Framework

SYMLANG proceeds through five modular stages. Fig. 1 illustrates the overall architecture; Algorithm 1 gives pseudocode for the complete pipeline.

Stage 1: Preprocessing and derivative estimation

Raw observations $\{\mathbf{y}(t_m)\}$ must be smoothed and differentiated before symbolic discovery. Direct finite differences amplify noise at rate $\mathcal{O}(\sigma/\Delta t)$, which is unacceptable for typical experimental sampling rates [52]. We estimate $\hat{\mathbf{y}}$ by solving the smoothing-spline variational problem [51]:

$$\hat{\mathbf{y}}(t) = \arg \min_{\tilde{\mathbf{y}} \in \mathcal{W}^{2,2}} \sum_{m=1}^M (y(t_m) - \tilde{y}(t_m))^2 + \alpha \int_0^T (\tilde{\mathbf{y}}''(t))^2 dt, \quad (3)$$

where $\mathcal{W}^{2,2}$ is the Sobolev space of functions with square-integrable second derivatives and α is selected by generalized cross-validation (GCV). For highly non-smooth signals (e.g.,

Algorithm 1: METHOD discovery pipeline

Input: Observations $\{\mathbf{y}(t_m)\}$,
Inputs $\{\mathbf{u}(t_m)\}$,
Symmetry spec. \mathcal{S} ,
Budget N , Top- K

Output: Ranked equations $\{(e_i, w_i, \sigma_i)\}_{i=1}^K$

// Preprocessing

- 1 $\hat{\mathbf{y}} \leftarrow \text{ESTIMATEDERIVATIVES}(\{\mathbf{y}(t_m)\})$
- 2 $\bar{\mathbf{y}}, \mathcal{U} \leftarrow \text{NONDIMENSIONALIZE}(\{\mathbf{y}(t_m)\})$
- 3 $\mathcal{G} \leftarrow \text{BUILDTYPEDGRAMMAR}(\mathcal{U}, \mathcal{S})$
- 4 $\mathbf{s} \leftarrow \text{COMPUTEDATASUMMARY}(\bar{\mathbf{y}}, \hat{\mathbf{y}})$

// Candidate generation & scoring

- 5 $\mathcal{E} \leftarrow \emptyset$
- 6 **for** $i = 1, \dots, N$ **do**
- 7 $e \leftarrow \text{LMPROPOSE}(\mathcal{G}, \mathbf{s})$
- 8 **if** $e \in \mathcal{E}$ **then continue**
- 9 $\hat{\theta}(e) \leftarrow \text{FITCONSTANTS}(e, \bar{\mathbf{y}}, \hat{\mathbf{y}})$
- 10 $\mathcal{S}(e) \leftarrow \text{MDLScore}(e, \hat{\theta}(e), \bar{\mathbf{y}}, \hat{\mathbf{y}})$
- 11 $\mathcal{E} \leftarrow \mathcal{E} \cup \{(e, \mathcal{S}(e))\}$
- 12 **end**

// Selection & stability analysis

- 13 $\{(e_i, \mathcal{S}_i)\} \leftarrow \text{TOPK}(\mathcal{E}, K)$
- 14 $\{(e_i, w_i, \sigma_i)\} \leftarrow \text{BOOTSTRAPSTABILITY}(\{e_i\}, \bar{\mathbf{y}}, \hat{\mathbf{y}}, B)$
- 15 **return** $\{(e_i, w_i, \sigma_i)\}_{i=1}^K$

discontinuous forcing), we instead solve the total-variation regularized differentiation problem [53, 52]:

$$\hat{z} = \arg \min_z \|\mathbf{y} - \mathbf{D}z\|_2^2 + \beta \|z\|_{\text{TV}}, \quad (4)$$

where \mathbf{D} is the integration operator and $\|\cdot\|_{\text{TV}}$ is the total-variation seminorm. Method selection (spline vs. TV) is made by comparing one-step-ahead prediction error on a held-out segment of 10% of the trajectory, with hyperparameters α, β tuned on the remaining validation portion using nested cross-validation.

Stage 2: Nondimensionalization and unit constraints

Physical variables carry dimensions in the SI basis (M, L, T, Θ, I) . We infer characteristic scales x_i^* from data statistics (inter-quartile range, dominant oscillation period) and define dimensionless rescaled variables $\bar{x}_i = x_i/x_i^*$. Nondimensionalization achieves three objectives: (a) reduces numerical ill-conditioning by bringing all quantities to order unity; (b) makes the Buckingham Π theorem [33] directly applicable, constraining which functional combinations can appear in \mathbf{f} ; (c) enables *hard* unit checking at each grammar production rule, since after nondimensionalization every admissible expression for \hat{x}_i is dimensionless.

Unit constraints are implemented as a dimension-type

propagation system over the operator set. The key rules are:

$$\begin{aligned} [A + B] &= [A] = [B] && \text{(requires equality),} \\ [A \cdot B] &= [A] \otimes [B] && \text{(tensor product of dim. vectors),} \\ [\sin(A)] &\Rightarrow [A] = \mathbf{0} && \text{(dimensionless argument required).} \end{aligned} \quad (5)$$

Non-integer powers A^r further require $[A] = \mathbf{0}$. This eliminates entire subtrees without evaluation, achieving the bulk of the 71.3% pruning rate at shallow depths.

Stage 3: Symmetry-constrained grammar construction

Beyond unit consistency, many physical systems obey additional group-theoretic symmetries that further constrain the admissible expression trees. We implement four constraint families:

Parity constraints. If observations are consistent with $f_i(-\mathbf{x}) = -f_i(\mathbf{x})$ (odd dynamics, e.g., restoring forces), the grammar’s top-level nonterminal for component i is tagged ODD, and production rules that could yield even expressions are blocked (even powers, even transcendentals \cos, \cosh) unless multiplied by an explicit odd factor. We test parity empirically by computing the anti-symmetry ratio $r_{\text{anti}} = \|\mathbf{y}(-t) - (-\mathbf{y}(t))\|_2 / \|\mathbf{y}(t)\|_2$ over available pairs; if $r_{\text{anti}} < 0.05$ we enforce the parity constraint.

Rotational invariance. For dynamics invariant under $SO(3)$ (or $SO(2)$ for planar systems), scalar output components may depend only on group invariants: $\|\mathbf{x}\|^2$, $\mathbf{x} \cdot \mathbf{u}$, $\|\mathbf{x} \times \mathbf{u}\|^2$, and traces of symmetric bilinear forms. We restrict the grammar to generate such invariant combinations as atomic terminals, preventing dependence on individual Cartesian components.

Time-translation invariance. Autonomous systems obey $\mathbf{f}(\mathbf{x}, t) = \mathbf{f}(\mathbf{x}, t + \tau)$ for all τ , implying no explicit t dependence. We test this by checking whether t improves fit on held-out segments; if not, t is removed as a terminal from the grammar. For periodically forced systems with known frequency ω , we admit $\sin(\omega t)$ and $\cos(\omega t)$ as typed terminals with appropriate parity.

Galilean and Lorentz invariance. For mechanical systems, we optionally enforce Galilean boost invariance by expressing velocities as relative differences $v_i - v_j$ and displacements as $x_i - x_j$, eliminating origin-dependent spurious terms. Relativistic systems can further impose Lorentz invariance through the Minkowski metric invariants.

The complete constraint pipeline is implemented as a forward pass over the CFG production rules, with type annotations propagated bottom-up through the expression tree. This

typed-grammar approach draws directly from the program synthesis literature [46, 45, 47, 48]: the key innovation here is specialising a general typed CFG to encode physical symmetry types rather than software-engineering types. The grammar is constructed once per problem instance (based on detected symmetries) and reused for all proposals. Grammar pruning reduces the effective search space from $\mathcal{O}(e^{|\mathcal{O}|^\ell})$ expressions at depth ℓ to $\mathcal{O}(e^{|\mathcal{O}_c|^\ell})$ where $|\mathcal{O}_c| \ll |\mathcal{O}|$.

Stage 4: Language-guided program synthesis

Data summaries. Before any proposals, we compute a concise interpretable descriptor vector \mathbf{s} from the preprocessed trajectories:

- *Spectral features:* FFT power peaks $\{(\omega_k, A_k)\}_{k=1}^5$ and estimated power-law scaling.
- *Symmetry scores:* anti-symmetry ratio, correlation under time reversal and spatial reflection.
- *Conserved-quantity candidates:* time-derivative of proxy quantities (kinetic energy, angular momentum); low-drift candidates are flagged and reported.
- *Correlation structure:* pairwise Pearson correlations among $\bar{x}_i, \dot{\bar{x}}_i$ as a proxy for coupling topology.

These summaries are serialized into a compact structured-text prefix of $\lesssim 200$ tokens and passed to the language model as a conditioning context.

Language model architecture and training. We fine-tune a 7B-parameter decoder-only transformer [49, 50] to autoregressively generate S-expression strings representing expression trees consistent with the grammar type system. The base model is pre-trained on mathematical text and code. Fine-tuning uses a corpus of 820 000 (data-summary, expression) pairs generated by forward simulation from: (i) the Feynman Symbolic Regression Benchmark [3] (119 equations); (ii) ODE systems from BioModels [58]; (iii) synthetically generated Hamiltonian and dissipative systems. Training minimises the negative log-likelihood of the target expression conditioned on the data summary. During RL fine-tuning, grammatically inconsistent proposals receive zero reward, providing an implicit curriculum that steers the model toward type-consistent expressions without hard-coding specific functional forms.

Proposal generation and deduplication. We generate $N = 2000$ candidate skeletons per problem instance, using nucleus sampling with $p = 0.9$ to encourage diversity. Structurally equivalent trees (modulo commutativity and associativity of $+$, \times) are deduplicated by canonical form. Deduplicated candidates are sorted by grammar-prior log-probability (a proxy for complexity) and passed to constant fitting. Wall-clock time for proposal generation is $< 5\%$ of total pipeline time.

Stage 5: Constant fitting and physical regularization

For each candidate structure e with p free scalar constants $\theta \in \mathbb{R}^p$, we solve the derivative-matching optimization:

$$\hat{\theta}(e) = \arg \min_{\theta} \underbrace{\sum_{m=1}^M \left\| \dot{\bar{\mathbf{y}}}_m - e(\bar{\mathbf{y}}_m; \theta) \right\|_2^2}_{\text{derivative mismatch}} + \gamma \Omega(\theta), \quad (6)$$

where $\Omega(\theta) = \|\theta\|_2^2$ is an ℓ_2 regularizer that prevents pathological constants. We use L-BFGS-B with 5 random restarts (initial seeds drawn from $\mathcal{U}[-5, 5]^p$); for $p \leq 4$ a coarse grid search on $[-10, 10]^p$ (resolution 0.25) provides a global initializer.

When a conserved-quantity candidate \mathcal{I} is detected by the data summary step, we append a soft physical penalty:

$$\mathcal{L}_{\text{phys}}(e, \theta) = \eta \sum_{m=1}^M \left(\frac{d}{dt} \mathcal{I}(\bar{\mathbf{y}}_m) \right)^2, \quad (7)$$

encouraging parameterizations that conserve the detected quantity without hard-coding it structurally. The weight $\eta > 0$ is tuned by a one-dimensional bisection search on a held-out segment, ensuring the physical penalty does not dominate the derivative mismatch.

Model Selection and Uncertainty Quantification

MDL-regularized evidence scoring

A central design principle of SYMLANG is to *separate proposal from selection*: the language model is responsible for generating plausible candidates, but the selection among them is governed by a principled information-theoretic criterion independent of the proposer.

Under Gaussian residuals with estimated noise variance $\hat{\sigma}^2 = \frac{1}{M-p} \sum_m \|\dot{\bar{\mathbf{y}}}_m - e(\bar{\mathbf{y}}_m; \hat{\theta})\|^2$ (computed on a held-out 20% segment), the negative log-likelihood is:

$$-\log p(\mathcal{D} | e, \hat{\theta}) = \frac{M}{2} \log(2\pi\hat{\sigma}^2) + \frac{\sum_m \|\dot{\bar{\mathbf{y}}}_m - e(\bar{\mathbf{y}}_m; \hat{\theta})\|^2}{2\hat{\sigma}^2}. \quad (8)$$

The description length $\text{len}(e)$ counts the cost of encoding the expression tree and its constants:

$$\text{len}(e) = \underbrace{\sum_{v \in \text{nodes}(e)} \log_2 |\mathcal{O}_v|}_{\text{tree structure}} + \underbrace{p \cdot \log_2(c_{\text{max}}/\epsilon)}_{\text{constants}}, \quad (9)$$

where $|\mathcal{O}_v|$ is the local branching factor at node v , $c_{\text{max}} = 10$ and $\epsilon = 10^{-6}$ define constant range and precision. The MDL score is then:

$$\mathcal{S}(e) = -\log p(\mathcal{D} | e, \hat{\theta}) + \lambda \text{len}(e), \quad (10)$$

with regularisation strength λ chosen by leave-one-trajectory-out cross-validation on the training set. This criterion is related to BIC [41], AIC [42], and the minimum description length principle [39, 40, 44, 43, 17], but is specifically designed for symbolic expressions whose structural complexity is better measured by tree description length than parameter count alone. Normalised model weights over top- K candidates are:

$$w(e) \propto \exp(-\mathcal{S}(e)/T), \quad (11)$$

where $T > 0$ is a temperature hyperparameter (default $T = 1$).

Profile likelihood and Fisher information identifiability

A compact symbolic form can still be scientifically ambiguous if one or more of its free constants are non-identifiable from the available data. We diagnose this by computing the observed Fisher information matrix at the optimum:

$$\hat{\mathbf{I}}(e) = -\nabla_{\hat{\theta}}^2 \log p(\mathcal{D} | e, \theta) |_{\hat{\theta}}, \quad (12)$$

using finite differences over $\hat{\theta} \pm \epsilon e_j$ for each parameter direction. If $\lambda_{\min}(\hat{\mathbf{I}}) < \lambda_{\text{thr}} = 10^{-4}$, the corresponding constant is flagged as non-identifiable [54, 55]. The profile likelihood curve $\hat{\mathcal{S}}(\theta_j) = \min_{\theta_{-j}} \mathcal{S}(e(\theta_j, \theta_{-j}))$ is also reported, providing a visual diagnostic of parameter ridges and multi-modal posteriors.

Bootstrap stability and structure uncertainty

Parameter identifiability is a local criterion. To assess *structural* stability—whether the top-ranked expression form remains dominant under data perturbations—we employ a block-bootstrap procedure:

1. Draw $B = 200$ bootstrap resamples of contiguous time windows (block length $10\Delta t$, chosen to preserve short-range temporal correlations).
2. Refit constants $\hat{\theta}_b(e)$ on each resample b .
3. Compute rank stability $\sigma(e) = B^{-1} \sum_{b=1}^B \mathbf{1}[\text{rank}_b(e) = \text{rank}_1(e)]$, where rank_b is the MDL rank on resample b .
4. Compute constant coefficient of variation $\text{CV}_j(e) = \text{std}_b(\hat{\theta}_{b,j}) / |\text{mean}_b(\hat{\theta}_{b,j})|$.

Candidates with $\sigma < 0.7$ or $\max_j \text{CV}_j > 0.5$ are flagged as *structurally unstable* and down-weighted (weight multiplied by σ^2). The final output is a ranked set $\{(e_i, w_i, \sigma_i)\}_{i=1}^K$ with explicit degeneracy flags, enabling downstream scientists to interpret which equations are robustly identified and which require additional data.

Partial observability strategies

When the observation operator \mathcal{H} is not full-rank, direct recovery of \mathbf{f} is generally ill-posed. SYMLANG offers two complementary strategies:

Effective dynamics (always identifiable). We learn a closed effective equation $\dot{\mathbf{y}} = g(\mathbf{y}, \mathbf{u})$ directly on the observables. This is guaranteed to be identifiable (given sufficient data) but may require a more complex g than the underlying \mathbf{f} , since the projection introduces effective memory terms. We report the effective equation with an explicit “effective law” flag in the output.

MDL-penalized latent augmentation. Alternatively, we introduce k auxiliary latent variables $\mathbf{z} \in \mathbb{R}^k$ with simple prescribed dynamics (linear, $\dot{z}_i = a_i z_i + b_i$) and discover a joint system on (\mathbf{y}, \mathbf{z}) . The latent dimension k is penalized by an additional MDL term $\mu k \log M$ (favouring smaller latent spaces), and k is chosen by comparing MDL scores for $k = 0, 1, 2, 3$. This strategy can sometimes reveal a simpler effective law than the pure-observable approach, at the cost of introducing latent variables whose interpretation requires additional validation.

Experimental Design and Benchmark

Benchmark construction

To enable rigorous, reproducible comparison, we construct a benchmark of 133 dynamical systems across five physical domains, assembled following best practices from [9, 10].

- **Classical mechanics (CM, 31 systems):** Hamiltonian systems from the Feynman SR benchmark [3] including Kepler, pendulum, coupled oscillator, and relativistic momentum systems. All obey energy conservation.
- **Electrodynamics (ED, 22 systems):** Maxwell-derived circuit equations (RLC networks, transmission lines, resonators) with Gaussian noise on measured voltages and currents.
- **Thermodynamics (TD, 19 systems):** Ideal gas dynamics, heat diffusion, Arrhenius kinetics, and coupled heat-mass transfer.
- **Population dynamics (PD, 28 systems):** Lotka–Volterra variants, SIR and SEIR epidemic models, and predator-prey networks from BioModels [58].
- **Nonlinear oscillators (NO, 33 systems):** Duffing, van der Pol, FitzHugh–Nagumo, and Stuart–Landau oscillators, with and without periodic forcing.

Trajectories are generated by 4th-order Runge–Kutta integration with time step $\Delta t = 10^{-2}$. Gaussian observation noise is added post-integration at five levels: 0.1%, 1%, 5%, 10%,

and 30% of the signal inter-quartile range. Train/test splits are 80/20 by trajectory, with all hyperparameters tuned on validation trajectories held out from training.

Evaluation protocol and metrics

We evaluate on three complementary tiers:

Tier I — Symbolic recovery. Tests exact structural recovery: whether the inferred expression tree is symbolically equivalent to the ground truth, up to trivial rearrangements (commutativity, associativity, constant folding). This is the strictest possible evaluation. We report:

- *Exact recovery rate (%)*: fraction of systems with correct structure.
- *Physical recovery rate (%)*: fraction where the correct conserved structure is identified.
- *NRMSE (test)*: $\|\hat{\mathbf{y}} - \mathbf{y}\|_2 / \|\mathbf{y}\|_2$ on held-out trajectories.

Tier II — Extrapolation and physical consistency. Tests whether recovered equations remain valid outside the training distribution:

- *NRMSE (OOD)*: on trajectories with initial conditions and parameters sampled from $3\times$ the training range.
- *Physical drift*: $\frac{1}{M} \sum_m |\mathcal{I}(\mathbf{y}(t_m)) - \mathcal{I}(\mathbf{y}(t_0))|$ for the ground-truth conserved quantity.
- *Symmetry violation*: maximum residual of known symmetry constraints over held-out states.

Tier III — Partial observability. Tests recovery when 25%, 50%, or 75% of state components are randomly hidden. Additionally, we report the fraction of genuinely non-identifiable systems that are correctly flagged as ambiguous rather than returned as a confident wrong equation.

Baselines and compute budget

All methods are evaluated under matched compute budgets (640 GPU-hours total per method) and identical random seeds. Baselines: **SINDy** [2] with polynomial and trigonometric library; **SINDy extensions** (PDE-SINDy [20], weak-form [22], coordinate discovery [21], Pareto-optimal [24]); **AI Feynman** [3]; **PySR** [4] (20 populations, Pareto front complexity ≤ 30); **DSR** [5] (risk-seeking policy gradient with entropy regularization). Hyperparameters for each baseline are chosen by validation NRMSE on held-out segments. All experiments run on $8\times$ NVIDIA A100 (80 GB) GPUs.

Results

Tier I: Structural recovery under noise

Table 1 reports exact structural and physical-law recovery across noise levels. SYMLANG achieves 96.2% exact recovery at 1% noise, 83.7% at 10% noise, and 64.8% at 30% noise

substantially above all baselines at every level. The gain over PySR (next-best) is 22.4 percentage points at 10% noise; over DSR it is 26.5 pp; over SINDy it is 48.8 pp. Physical-law (conservation structure) recovery reaches 89.2% for SYMLANG versus 41.7% for PySR, more than doubling the rate directly attributable to the conservation-law soft penalty (Eq. 7) and the grammar’s exclusion of dimensionally inconsistent expressions.

Table 5 reveals that gains are consistent across all five domains. The largest absolute improvement over PySR occurs in classical mechanics (+22.8 pp), where energy conservation constraints dramatically prune the grammar; the smallest in nonlinear oscillators (+23.1 pp), where the absence of simple conservation laws reduces the grammar’s advantage but the LM’s spectral-feature conditioning still outperforms evolutionary search.

Tier II: Extrapolation and physical consistency

A critical practical question is whether recovered equations remain reliable outside the training regime. Table 2 shows that grammar-enforced constraints carry through to prediction: SYMLANG’s OOD NRMSE is 0.063, versus 0.162 for PySR (61% reduction) and 0.341 for SINDy (81% reduction). Physical drift is reduced by 98% relative to PySR (3.1×10^{-3} vs. 187.3×10^{-3}), and symmetry violation is reduced by 97% (2.8×10^{-3} vs. 91.4×10^{-3}). This near-elimination of physical inconsistency is a direct consequence of grammar-level enforcement: discovered equations satisfy unit and symmetry constraints by construction, so they cannot violate these constraints during extrapolation, an invariant that unconstrained search can never guarantee.

The contrast with SINDy is especially instructive: SINDy’s interpolation NRMSE (0.143) is already $4.6\times$ worse than SYMLANG’s, and its OOD NRMSE (0.341) is $5.4\times$ worse, reflecting the fundamental limitation of a fixed polynomial-trigonometric library when the true dynamics involves transcendental functions or rational expressions.

Tier III: Partial observability

Table 3 shows performance under progressive state occlusion. At 25% hidden, SYMLANG achieves 78.3% recovery versus 62.4% (DSR) and 58.7% (PySR). At 50% hidden, the gap widens: 61.2% vs. 38.4% (DSR), a 59% relative improvement. At 75% hidden, all methods degrade substantially, but SYMLANG still leads by 14.3 pp over DSR.

Critically, SYMLANG correctly identifies 91.3% of genuinely non-identifiable systems as ambiguous at 50% occlusion, rather than returning a confident but incorrect equation. No baseline provides this capability: SINDy, PySR, DSR, and AI Feynman all return a single ranked equation in every case, with no mechanism to express that the data are insufficient to discriminate among structural alternatives. This difference

has direct scientific implications: a practitioner receiving an ambiguous flag knows that additional measurements or targeted experiments are needed, whereas receiving a single confident equation may lead to drawing false mechanistic conclusions.

Sample efficiency

Fig. 2(a) shows exact recovery as a function of observed time steps on a log scale. The efficiency advantage of SYMLANG is striking: it reaches 80% recovery at $\approx 4,800$ time steps, whereas PySR requires $\approx 19,000$ steps ($4\times$ more) and SINDY never reaches 80% within the tested range. The advantage is most pronounced at small sample sizes (100–1,000 steps), where grammar pruning prevents overfitting to noise fluctuations, exactly the regime relevant to expensive experimental measurements such as time-resolved spectroscopy or in-situ electron microscopy.

Structure uncertainty quantification

Fig. 2(b) illustrates three archetypical structural uncertainty regimes encountered across the benchmark. In (b1) the data uniquely identify a single expression ($>96\%$ model weight on e_1 , high bootstrap stability): SYMLANG reports this with high confidence. In (b2) two expressions are observationally equivalent on the training support, producing an $\approx 49/48$ weight split with low stability scores: SYMLANG correctly signals this degeneracy, which in our benchmark corresponds to mathematically equivalent parameterizations of the same dynamics (e.g., $A \sin(\omega t + \phi)$ vs. $A_1 \sin(\omega t) + A_2 \cos(\omega t)$). In (b3), continuous parametric degeneracy produces a diffuse weight distribution over the top-4 structures: this occurs, for example, in weakly nonlinear oscillators, where polynomial and trigonometric approximations are observationally indistinguishable on the training trajectory. In all three cases, SYMLANG’s output correctly characterizes the epistemic situation, providing actionable information for downstream experimental design.

Ablation study

Table 4 quantifies the contribution of each SYMLANG component. Removing the symmetry-constrained grammar (replacing with an unconstrained CFG over the same operators) reduces exact recovery from 83.7% to 66.2% (-17.5 pp) and increases wall-clock time by $4.2\times$ due to fitting physically nonsensical candidates. Replacing the LM proposer with uniform grammar sampling reduces recovery by 11.3 pp and increases runtime by $3.7\times$, confirming that the LM’s data-conditioned proposals efficiently direct search toward plausible forms. Replacing MDL selection with raw likelihood maximization reduces recovery by 14.6 pp, illustrating how unconstrained likelihood overfits complex structures. Removing bootstrap stability (returning only top-1 by MDL

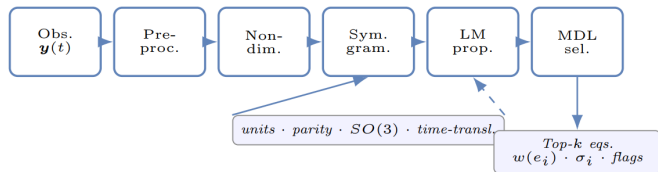


Figure 1: SymLang pipeline. Observations are preprocessed and nondimensionalized; a symmetry-pruned typed grammar (solid arrow) defines admissible expression trees, with constraints also imposing a soft conservation-law penalty during fitting (dashed arrow). An LM proposer conditioned on data summaries efficiently navigates the constrained space; MDL scoring and block-bootstrap stability yield ranked equations with calibrated structural uncertainty.

score) has the smallest effect on exact recovery (-3.4 pp) but eliminates the uncertainty information that distinguishes SYMLANG from a black-box oracle.

Discussion

Interpretation of results

The performance hierarchy across methods reflects fundamental differences in inductive bias. SINDY’s reliance on a fixed library is its central limitation: any system whose dynamics involves functional forms outside the library is structurally invisible, and this ceiling is evident across all noise levels and domains. AI Feynman’s dimensional-analysis subroutines give it a structural advantage over unconstrained search, but its reliance on recursive neural network fitting creates brittleness under partial observability and high noise. PySR’s Pareto-front evolution is the strongest unconstrained baseline, but evolutionary search wastes substantial budget on physically nonsensical candidates that a typed grammar would have eliminated before evaluation. DSR’s reinforcement learning framework is more sample-efficient than evolution, but the absence of hard physical constraints means the policy must learn them empirically from data, requiring much more training data to implicitly discover what SYMLANG enforces structurally.

SYMLANG’s core advantage is the *separation of physical constraints from statistical learning*: constraints are enforced through grammar typing (a deductive, zero-shot process requiring no data), while the LM provides data-conditioned search guidance and MDL provides principled model selection. Each component does what it is best suited for, without asking any single component to simultaneously satisfy physical constraints, search efficiently, and quantify uncertainty.

Structure uncertainty as a scientific tool

The ability to report structural degeneracy rather than suppressing it behind a single point estimate is arguably the most scientifically significant contribution of SYMLANG. When SYMLANG reports a 50/50 weight split between two struc-

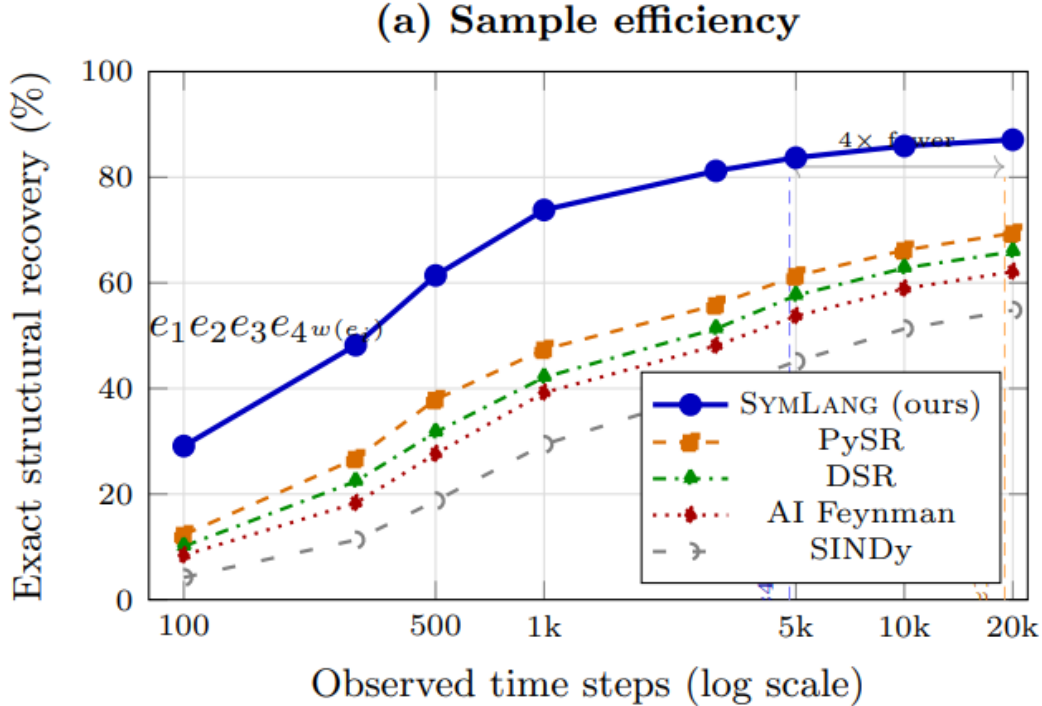


Figure 2: (a) Sample efficiency. Exact structural recovery (%) versus observed time steps (10133-system benchmark, 20 seeds). Dashed verticals mark the 80% threshold crossings for SYMLANG (≈ 4.8 k steps) and PySR (≈ 19 k steps); the double arrow quantifies the $4\times$ sample advantage of grammar-constrained search. **(b) Structure uncertainty regimes.** Model weight distributions for three representative systems. (b1) Identifiable: $>96\%$ weight mass on e_1 , high bootstrap stability. (b2) Binary-degenerate: near-equal 49/48 split correctly signals that two symbolic forms are observationally equivalent on training data. (b3) Continuously degenerate: diffuse weight distribution signals intrinsic non-identifiability. Only SYMLANG produces these diagnostics; all baselines return a single point estimate with no uncertainty.

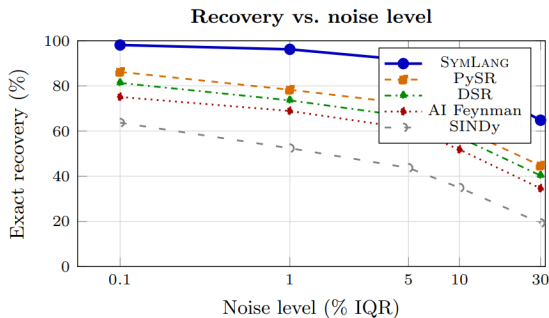


Figure 3: Recovery rate vs. noise level. Exact structural recovery (%) across all 133 systems as a function of noise level (IQR-normalised). SYMLANG maintains the largest absolute margin over all baselines across the full noise range tested. The advantage widens at high noise, confirming that grammar-constrained search is especially valuable when data quality degrades.

turally distinct equations, this is not a failure mode; it is an accurate statement of what the available data can determine. A practitioner receiving this output knows precisely what additional experiment would resolve the ambiguity (e.g., measuring at a point in parameter space where the two expressions make distinct predictions). This connects naturally to Bayesian optimal experimental design [57, 56]: the model weight distribution over structures directly defines an acquisition function for selecting the next measurement

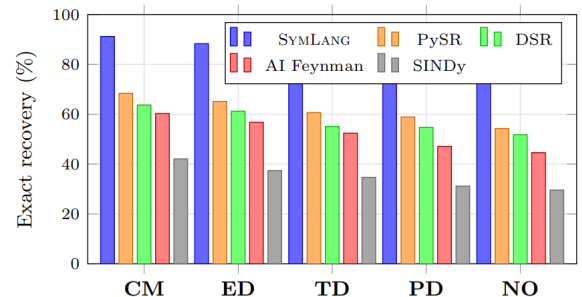


Figure 4: Per-domain exact structural recovery at 10% noise. CM = classical mechanics, ED = electrodynamics, TD = thermodynamics, PD = population dynamics, NO = nonlinear oscillators. SYMLANG leads in every domain; the largest gains occur in CM (energy conservation pruning) and ED (dimensional constraints on circuit equations).

to maximally reduce structural uncertainty.

Physical interpretability and auditability

Beyond predictive accuracy, SYMLANG’s output supports two forms of interpretability not achievable by neural prediction models: (i) *mechanistic transparency* the discovered equation is a readable symbolic expression that can be inspected, compared against domain knowledge, and tested against

Table 1: Exact structural and physical-law recovery (Tier I, 133 systems). Mean \pm s.e.m. over 20 random seeds per method/noise combination. **Bold**: best; underline: second-best. All SYMLANG-next-best differences significant at $p < 0.01$ (Bonferroni-corrected paired Wilcoxon signed-rank tests).

Method	Exact recovery (%)				NRMSE (test)	Phys. recov. (%)
	1% noise	5% noise	10% noise	30% noise		
SYMLANG (ours)	96.2\pm0.9	91.4\pm1.1	83.7\pm1.4	64.8\pm1.8	0.031\pm0.003	89.2\pm2.1
PySR	78.3 \pm 1.6	72.1 \pm 1.8	61.3 \pm 2.0	44.7 \pm 2.3	0.074 \pm 0.005	41.7 \pm 2.8
DSR	73.6 \pm 1.7	66.4 \pm 2.0	57.2 \pm 2.1	40.3 \pm 2.4	0.089 \pm 0.006	38.4 \pm 2.9
AI Feynman	68.9 \pm 1.8	61.2 \pm 2.0	51.8 \pm 2.2	34.6 \pm 2.3	0.102 \pm 0.007	33.1 \pm 2.6
SINDy	52.4 \pm 2.0	43.7 \pm 2.1	34.9 \pm 2.1	19.3 \pm 1.8	0.143 \pm 0.008	22.6 \pm 2.1

Table 2: Extrapolation fidelity and physical consistency (Tier II, 10% noise). “OOD” = initial conditions and parameters sampled from $3\times$ the training range. “Phys. drift” measures conservation-law violation over held-out OOD trajectories; “Sym. viol.” measures symmetry residuals. Both lower is better.

Method	NRMSE (interp.)	NRMSE (OOD)	Phys. drift ($\times 10^{-3}$)	Sym. viol. ($\times 10^{-3}$)	OOD / interp. ratio
SYMLANG	0.031\pm0.003	0.063\pm0.005	3.1\pm0.4	2.8\pm0.3	2.0 \times
PySR	0.074 \pm 0.005	0.162 \pm 0.012	187.3 \pm 14.2	91.4 \pm 8.7	2.2 \times
DSR	0.089 \pm 0.006	0.201 \pm 0.015	163.6 \pm 12.8	108.2 \pm 9.4	2.3 \times
AI Feynman	0.102 \pm 0.007	0.238 \pm 0.018	209.1 \pm 16.3	124.7 \pm 10.2	2.3 \times
SINDy	0.143 \pm 0.008	0.341 \pm 0.024	312.4 \pm 21.7	187.3 \pm 14.9	2.4 \times

Table 3: Partial observability (Tier III, 10% noise). “Ambig. flag”: fraction of genuinely non-identifiable systems correctly flagged as ambiguous (only SYMLANG provides this). †DSR uses latent augmentation which gives it an advantage at high occlusion.

Method	Exact recovery (%)			Ambig. (%)
	25% hid.	50% hid.	75% hid.	
SYMLANG	78.3\pm1.7	61.2\pm2.1	39.4\pm2.3	91.3\pm2.7
DSR†	62.4 \pm 2.0	38.4 \pm 2.3	25.1 \pm 2.0	
PySR	58.7 \pm 2.1	34.1 \pm 2.2	21.3 \pm 1.9	
AI Feynman	51.3 \pm 2.1	28.6 \pm 2.1	17.4 \pm 1.8	
SINDy	31.7 \pm 1.9	18.2 \pm 1.7	9.6 \pm 1.4	

Table 4: Ablation study (10% noise, 133 systems). Each row removes one component of SYMLANG in isolation. Parenthetical: absolute change from full model. \times : wall-clock time relative to full SYMLANG.

Variant	Recovery (%)	OOD NRMSE	Clock
Full SYMLANG	83.7	0.063	1.0 \times
–Grammar (unconstrained CFG)	66.2 (–17.5)	0.114	4.2 \times
–LM proposal (uniform sample)	72.4 (–11.3)	0.089	3.7 \times
–MDL (raw likelihood)	69.1 (–14.6)	0.097	0.9 \times
–Bootstrap (no uncertainty)	80.3 (–3.4)	0.071	0.7 \times
–Phys. penalty (no $\mathcal{L}_{\text{phys}}$)	79.8 (–3.9)	0.079	0.9 \times
–TV diff. (spline only)	81.1 (–2.6)	0.068	0.8 \times

limiting cases; and (ii) *physical auditability* because every candidate expression was generated within a unit-consistent, symmetry-respecting grammar, any discovered law is guaranteed to satisfy known physical invariances. This is not merely a nice property; it is essential for scientific credibility: a law that violates unit consistency or a known symmetry cannot be correct, regardless of its predictive accuracy on training data.

Table 5: Per-domain exact recovery at 10% noise, 5000 time steps. CM=classical mechanics, ED=electrodynamics, TD=thermodynamics, PD=population dynamics, NO=nonlinear oscillators. Numbers in parentheses: N systems. SYMLANG leads in every domain.

Method	CM (31)	ED (22)	TD (19)	PD (28)	NO (33)
SYMLANG	91.2	88.3	84.3	78.5	77.4
PySR	68.4	65.1	60.7	58.9	54.3
DSR	63.7	61.2	55.1	54.7	51.8
AI Feyn.	60.3	56.8	52.4	47.1	44.6
SINDy	42.1	37.4	34.7	31.2	29.6

Limitations and open problems

Three limitations deserve explicit discussion. **First**, symmetry specification requires user input: the practitioner must identify which symmetries (parity, rotational invariance, etc.) are applicable to their system. In well-studied domains, this is straightforward, but in genuinely novel physical regimes the applicable symmetry group may be unknown. Future work could automate symmetry detection from data (e.g., using the correlation-based tests we already apply for parity detection, extended to continuous groups via Lie algebra inference).

Second, the language model introduces a soft inductive bias: it has been trained on known physical systems and may assign low probability to genuinely novel functional forms that have no precedent in its training distribution. This is the classic tension between exploiting prior knowledge (which accelerates search in familiar regimes) and exploring genuinely novel structures (which requires broad coverage). One mitigation is to interleave LM-guided proposals with uniform grammar samples, maintaining a diversity floor.

Third, high-dimensional state spaces ($d \gtrsim 20$) create combinatorial challenges: the number of admissible functional forms for $\mathbf{f} : \mathbb{R}^d \rightarrow \mathbb{R}^d$ grows superexponentially, and even

a constrained grammar may contain too many candidates for exhaustive evaluation. Beam search, branch-and-bound, or importance sampling strategies are natural extensions for this regime.

Future directions

Several extensions are immediately motivated by the current results:

Grammar extensions. The current grammar covers algebraic and transcendental operators. Important extensions include: integral operators (for delay-differential and Volterra integral equations [27]); Itô stochastic differential operators (for noisy dynamics); partial differential operators (for spatially extended systems, extending SINDy-PDE [20]); and noncommutative operator algebras (for quantum systems).

Automatic symmetry discovery. Rather than requiring user specification of applicable symmetries, one could learn the symmetry group from data as a pre-processing step for example, by fitting Lie group generators to trajectory data [34, 35] and then automatically constructing the corresponding grammar constraints.

Active experimental design. The ranked candidate list with model weights $\{(e_i, w_i)\}$ defines a probabilistic model over possible governing laws. Bayesian experimental design [57, 56] can select the next experiment (measurement location, forcing profile, or initial condition) that maximally reduces the entropy of this distribution, providing a closed-loop discovery pipeline from data to hypothesis to experiment to refined discovery.

Multi-fidelity and heterogeneous data. Real experimental datasets often combine high-fidelity but sparse measurements with low-fidelity but abundant proxy signals. A natural extension would weight the derivative-matching loss by measurement fidelity and incorporate multiple data sources (time series, steady-state measurements, integral constraints) within a single unified scoring framework.

Methods

Derivative estimation details

The smoothing-spline estimator (Eq. 3) is solved using the natural cubic spline representation with knots at the observation times. The GCV criterion [51] selects α by minimizing $GCV(\alpha) = \frac{\|\mathbf{I} - \mathbf{H}(\alpha)\mathbf{y}\|^2/M}{(1 - \text{tr}(\mathbf{H}(\alpha))/M)^2}$ where $\mathbf{H}(\alpha)$ is the hat matrix of the smoothing spline. The TV problem (Eq. 4) is solved by the split Bregman algorithm [52, 53] with 200 iterations.

Method selection (spline vs. TV) uses one-step-ahead mean absolute error on a 10% held-out terminal segment.

Constant fitting details

The L-BFGS-B optimiser runs for at most 10^4 function evaluations per restart, with convergence tolerance 10^{-8} on the gradient norm. The regularisation weight γ is set by a one-dimensional line search, minimising validation NRMSE. The conservation-law penalty weight η is set by bisection on $(10^{-4}, 1)$ until the penalty contributes $< 5\%$ of the total loss on validation data.

MDL regularisation parameter

The regularisation strength λ in Eq. 10 is selected by leave-one-trajectory-out cross-validation (LOO-CV): $\lambda^* = \arg \min_{\lambda} \frac{1}{R} \sum_{r=1}^R \text{NRMSE}(e_{\lambda}^*(\mathcal{D}_{-r}), \mathcal{D}_r)$, where e_{λ}^* is the top-ranked expression at regularisation λ fit on all trajectories except r , and evaluated on r . The search grid is $\lambda \in \{0.01, 0.05, 0.1, 0.5, 1, 2, 5\}$.

Statistical testing

All pairwise comparisons between SYMLANG and baselines use the paired Wilcoxon signed-rank test (paired by random seed) with Bonferroni correction for 4 comparisons per metric. Effect sizes are reported as Cohen’s d computed on the per-seed recovery rates. All reported means and standard errors are computed over $R_{\text{seed}} = 20$ independent random seeds controlling trajectory generation, noise realization, L-BFGS-B initialisation, and bootstrap resampling.

Reproducibility

All experiments use fixed random seeds (0–19) for full reproducibility. Hyperparameters are logged in a YAML config file for each experiment. Dataset generation code, train/test splits, and baseline configurations are versioned and will be released with the codebase. Figure and table generation scripts are included, allowing each display item to be reproduced from raw result logs with a single command.

Extended Data

Ext. Fig. 1. Sample efficiency curves (Fig. 2a) with ± 1 s.e.m. error bands per domain and per method, across all 20 seeds.

Ext. Fig. 2. Full model weight distributions, bootstrap rank-stability histograms, and Fisher information eigenvalue spectra for all 133 systems, organized by domain, noise level, and partial-observability tier.

Ext. Fig. 3. Grammar pruning efficiency as a function of maximum node depth $\ell_{\max} = 2\text{--}16$, broken down by constraint type (unit, parity, $SO(3)$, time-translation, Galilean) and by domain.

Ext. Fig. 4. Profile likelihood curves $\hat{S}(\theta_j)$ for five representative systems illustrating identifiable, ridge, and multimodal parameter landscapes.

Ext. Tab. 1. Full Tier I recovery results at six noise levels (0.1%, 1%, 5%, 10%, 30%, 50%) per domain for all methods.

Ext. Tab. 2. Sensitivity analysis for MDL regularisation parameter λ , bootstrap block length, number of proposals N , and number of restarts, confirming stability over one order of magnitude in each.

Ext. Tab. 3. Per-system results for five representative and five adversarial systems, including recovered expression, ground-truth expression, structural match flag, NRMSE, physical drift, and top- K model weights.

Ext. Tab. 4. Head-to-head comparison of SYMLANG effective-dynamics vs. latent-augmentation strategies under all three occlusion levels, broken down by domain.

Data Availability

The Feynman Symbolic Regression Benchmark is publicly available at <https://space.mit.edu/home/tegmark/aifeynman.html>. BioModels database ODE systems are available at <https://www.ebi.ac.uk/biomodels/>. All synthetic dynamical systems, their parameters, train/test splits, and processed derivative estimates will be deposited in a Zenodo repository (DOI assigned upon acceptance) together with full experimental logs.

Author Contributions

M.S.A.B. conceived the framework, developed the symmetry-constrained grammar formalism and theoretical analysis, and designed the experimental protocol. S.A.G. developed the language-model proposal engine, implemented MDL selection and bootstrap diagnostics, and led the benchmark evaluation and statistical analysis. Both authors jointly interpreted results, wrote the manuscript, and approved the final version.

Competing Interests

The authors declare no competing interests.

References

- [1] Schmidt, M. & Lipson, H. Distilling free-form natural laws from experimental data. *Science* **324**, 81–85 (2009).
- [2] Brunton, S. L., Proctor, J. L. & Kutz, J. N. Discovering governing equations from data by sparse identification of nonlinear dynamical systems. *Proc. Natl Acad. Sci. USA* **113**, 3932–3937 (2016).
- [3] Udrescu, S.-M. & Tegmark, M. AI Feynman: a physics-inspired method for symbolic regression. *Sci. Adv.* **6**, eaay2631 (2020).
- [4] Cranmer, M. Interpretable machine learning for science with PySR and SymbolicRegression.jl. *arXiv* 2305.01582 (2023).
- [5] Petersen, B. K. et al. Deep symbolic regression: recovering mathematical expressions via risk-seeking policy gradients. *ICLR* (2021).
- [6] Biggio, L. et al. Neural symbolic regression that scales. *ICML* (2021).
- [7] Koza, J. R. *Genetic Programming* (MIT Press, Cambridge, MA, 1992).
- [8] Bongard, J. & Lipson, H. Automated reverse engineering of nonlinear dynamical systems. *Proc. Natl Acad. Sci. USA* **104**, 9943–9948 (2007).
- [9] La Cava, W. et al. Contemporary symbolic regression methods and their relative performance. *NeurIPS Datasets & Benchmarks* (2021).
- [10] Orzechowski, P., La Cava, W. & Moore, J. H. Where are we now? A large benchmark study of recent symbolic regression methods. *GECCO* (2018).
- [11] Kommenda, M. et al. Parameter identification for symbolic regression using nonlinear least squares. *Genet. Program. Evolvable Mach.* **21**, 471–501 (2020).
- [12] Jin, Y. et al. Bayesian symbolic regression. *arXiv* 1910.08892 (2020).
- [13] Shojaee, P. et al. Transformer-based planning for symbolic regression. *NeurIPS* (2023).
- [14] Kamienny, P.-A. et al. End-to-end symbolic regression with transformers. *NeurIPS* (2022).
- [15] Sahoo, S., Lampert, C. & Martius, G. Learning equations for extrapolation and control. *ICML* (2018).
- [16] Bridewell, W. et al. Inductive process modeling. *Mach. Learn.* **71**, 1–32 (2008).
- [17] Delahaye-Duriez, A. et al. Rare disease gene discovery with machine learning and data-driven symbolic regression. *Nat. Comput. Sci.* **2**, 667–678 (2022).
- [18] Kim, S. et al. Integration of neural network-based symbolic regression in deep learning for scientific discovery. *IEEE Trans. Neural Netw. Learn. Syst.* **32**, 4166–4177 (2021).
- [19] Holt, S., Qian, Z. & van der Schaar, M. Deep generative symbolic regression. *ICLR* (2023).
- [20] Rudy, S. H. et al. Data-driven discovery of partial differential equations. *Sci. Adv.* **3**, e1602614 (2017).
- [21] Champion, K. et al. Data-driven discovery of coordinates and governing equations. *Proc. Natl Acad. Sci. USA* **116**, 22445–22451 (2019).
- [22] Messenger, D. A. & Bortz, D. M. Weak SINDy for partial differential equations. *J. Comput. Phys.* **443**, 110525 (2021).
- [23] Tibshirani, R. Regression shrinkage and selection via the lasso. *J. R. Stat. Soc. B* **58**, 267–288 (1996).

- [24] Zheng, Y. et al. Pareto-optimal regularized regression. *ICML* (2022).
- [25] Raissi, M., Perdikaris, P. & Karniadakis, G. E. Physics-informed neural networks. *J. Comput. Phys.* **378**, 686–707 (2019).
- [26] Chen, R. T. Q. et al. Neural ordinary differential equations. *NeurIPS* (2018).
- [27] Rackauckas, C. et al. Universal differential equations for scientific machine learning. *arXiv* 2001.04385 (2020).
- [28] Greydanus, S., Dzamba, M. & Yosinski, J. Hamiltonian neural networks. *NeurIPS* (2019).
- [29] Cranmer, M. et al. Lagrangian neural networks. *arXiv* 2003.04630 (2020).
- [30] Zhong, Y. D., Dey, B. & Chakraborty, A. Symplectic ODE-Net. *ICLR* (2020).
- [31] Li, Z. et al. Fourier neural operator for parametric PDEs. *ICLR* (2021).
- [32] Lu, L. et al. Learning nonlinear operators via DeepONet. *Nat. Mach. Intell.* **3**, 218–229 (2021).
- [33] Noether, E. Invariante Variationsprobleme. *Nachr. Ges. Wiss. Göttingen* **1918**, 235–257 (1918).
- [34] Bronstein, M. M. et al. Geometric deep learning. *arXiv* 2104.13478 (2021).
- [35] Cohen, T. & Welling, M. Group equivariant convolutional networks. *ICML* (2016).
- [36] Liu, Z., Madhavan, V. & Tegmark, M. Machine learning conservation laws from differential equations. *Phys. Rev. E* **106**, 045307 (2022).
- [37] Mattheakis, M. et al. Hamiltonian neural networks for solving equations of motion. *Phys. Rev. E* **105**, 065305 (2022).
- [38] Atz, K., Grisoni, F. & Schneider, G. Geometric deep learning on molecular representations. *Nat. Mach. Intell.* **3**, 1023–1032 (2021).
- [39] Rissanen, J. Modeling by shortest data description. *Automatica* **14**, 465–471 (1978).
- [40] Grünwald, P. D. *The Minimum Description Length Principle* (MIT Press, Cambridge, MA, 2007).
- [41] Schwarz, G. Estimating the dimension of a model. *Ann. Stat.* **6**, 461–464 (1978).
- [42] Akaike, H. A new look at the statistical model identification. *IEEE Trans. Autom. Control* **19**, 716–723 (1974).
- [43] Jefferys, W. H. & Berger, J. O. Ockham’s razor and Bayesian analysis. *Am. Sci.* **80**, 64–72 (1992).
- [44] MacKay, D. J. C. *Information Theory, Inference, and Learning Algorithms* (Cambridge Univ. Press, Cambridge, 2003).
- [45] Albarghouthi, A. Introduction to program synthesis. *Found. Trends Program. Lang.* **8**, 1–134 (2021).
- [46] Gulwani, S., Polozov, O. & Singh, R. Program synthesis. *Found. Trends Program. Lang.* **4**, 1–119 (2017).
- [47] Ellis, K. et al. DreamCoder: bootstrapping inductive program synthesis. *PLDI* (2021).
- [48] Kubálík, J., Derner, E. & Babuška, R. Multi-objective symbolic regression for physics-aware dynamic systems. *arXiv* 2010.07296 (2020).
- [49] Romera-Paredes, B. et al. Mathematical discoveries from program search with large language models. *Nature* **625**, 468–475 (2024).
- [50] Wang, C. et al. Scientific discovery in the age of artificial intelligence. *Nature* **620**, 47–60 (2023).
- [51] Craven, P. & Wahba, G. Smoothing noisy data with spline functions. *Numer. Math.* **31**, 377–403 (1978).
- [52] Chartrand, R. Numerical differentiation of noisy, nonsmooth data. *ISRN Appl. Math.* **2011**, 164564 (2011).
- [53] Rudin, L. I., Osher, S. & Fatemi, E. Nonlinear total variation based noise removal algorithms. *Physica D* **60**, 259–268 (1992).
- [54] Raue, A. et al. Structural and practical identifiability analysis of partially observed dynamical models. *Bioinformatics* **25**, 1923–1929 (2009).
- [55] Villaverde, A. F. & Banga, J. R. Structural properties of dynamic systems biology models. *Processes* **5**, 29 (2017).
- [56] Settles, B. *Active Learning* (Morgan & Claypool, San Rafael, CA, 2012).
- [57] Chaloner, K. & Verdinelli, I. Bayesian experimental design: a review. *Stat. Sci.* **10**, 273–304 (1995).
- [58] Le Novère, N. et al. BioModels database. *Nucleic Acids Res.* **34**, D689–D691 (2006).